Supporting Information

Kotar et al. 10.1073/pnas.0912455107

SI Text

Materials and Methods. ***Materials.*** Silica beads of radius $a = 1.5$ μm (BangsLabs) are suspended in a solution of glycerol 59wt% in ultrapure water, prefiltered through a 0.2 μm membrane, having a viscosity $\eta = (7.4 \pm 0.9) \times 10^{-3}$ Pa s at $T = 25$°C. The uncertainty is the std over all the measurements. The sample is sealed in a 150 μm thick cell, sandwiched between a microscope slide and cover slip.

Experimental protocol. The measurements are performed at the midheight in the sample, over 20 particle diameters from the top and bottom surfaces. Video analysis is done by correlation filtering with an optimized kernel, followed by 2D least square fitting to determine the particle position with subpixel resolution. This process is done on each video frame, at 100 frames per second, using custom software written in C. The computer used is a multicore and multiprocessor server PC running Linux with RT PREEMPT patch, making it capable of real-time operation.

Laser power (wavelength 1,064 nm) at the sample is around 160mW, divided between two traps, giving trap stiffness $\kappa = (1.55 \pm 0.07) \times 10^{-6}$ N/m. The optical trap is described in more detail in ref. 1. Around 5 min of video (30,000 frames) are taken as calibration, to measure trap strength (from position distribution) and sample viscosity (from autocorrelation time). Then, approximately 30 min of data (180,000 frames) are acquired with the position feedback activated, enforcing the geometric switch described above. Runs are started from inphase particle positions.

Calibration. The trap stiffness κ is determined by fitting the distribution of particle positions in the trap with $P(x) = Ae^{\frac{\kappa(x-x_0)^2}{2kT}}$, where $T = 25$°C. The viscosity η is determined by fitting the time autocorrelation function of the positions, with $g(t) = Ae^{\frac{-t}{\tau_0}} + B$, giving $\eta = \frac{\kappa t}{6\pi r}$.

Data analysis. The phase correlation is quantified using the parameter

$$Q_j = -\frac{\sum_{i=jn}^{(j+1)n} x_1(t_i)x_2(t_i)}{\sqrt{\sum_{i=jn}^{(j+1)n} x_1(t_i)^2 \sum_{i=jn}^{(j+1)n} x_2(t_i)^2}}, \qquad [S1]$$

where $n = 110$ frames (approximately three periods of oscillation). This order parameter is $Q = 0$ for uncorrelated signals, $Q = 1$ for motions in antiphase, and $Q = -1$ for inphase. The distribution of Q_j is obtained running the window over the entire experiment.

The delay time $\delta\tau_d$ is obtained by finding the local maximum of

$$Q_{j,k} = -\frac{\sum_{i=jn}^{(j+1)n} x_1(t_i)x_2(t_{i+k})}{\sqrt{\sum_{i=jn}^{(j+1)n} x_1(t_i)^2 \sum_{i=jn}^{(j+1)n} x_2(t_{i+k})^2}} \qquad [S2]$$

as a function of the lag k.

Numerical simulation. The equations of motion (see main text) are integrated numerically using a timestep equivalent to $1/400,000$ s. Thermal noise is generated following the procedure outlined in ref. 2. The algorithm has been coded in the C language, and tested extensively by verifying that fluctuation amplitude, autocorrelation function of single beads, and the cross-correlation function of two beads in stationary traps, all agree with experimental data from our lab and with the published results of ref. 3.

Numerical simulation allows to change some parameters that are fixed or difficult to access experimentally. The most important of these is the feedback time, which is set in the experiment by the time required for image analysis. Experimentally it can be made longer, but not any shorter than 0.01 s as in this work. In numerical simulation on the other hand, the feedback time is introduced artificially as the time interval between "observations" of the bead positions, i.e. the choice of moving (or maintaining fixed) each potential is made every feedback time. This can be as short as the numerical integration time.

Numerical simulation proves that feedback time is not important for any of the features in this work, but for consistency with the experiments (except where explicitly labeled differently) all simulation results in the main text are done at feedback time of 0.01 s, equivalent to the experiments. The most delicate point where one could be concerned of an effect of feedback time is with respect to Δt. Fig. S4 shows that the observed delay Δt is not an artifact of the feedback time of the system: a finite delay time is found for any feedback time that is implemented in the numerical simulation. Only very a long feedback time, much higher than in the experimental work, affects the results.

The other parameters which are simpler to change in the simulation than in the experiment are temperature and viscosity. Experimentally the problem is that these variables are coupled together (viscosity has a strong temperature dependence) and are also coupled to other experimental parameters (the trap stiffness depends on the difference in index of refraction between particles and solvent, and the latter changes on addition of viscosity modifiers).

For these parameters, again we investigated the behavior of the stochastic difference in switch times Δt. Numerical data showing the trends with temperature and viscosity are shown in Fig. S5. The behavior with temperature is particularly revealing for $T \to 0$, showing that also $\Delta t \to 0$, in agreement with the analytical solution that predicts exactly antiphase motion.

Analytical Results on the Synchronized State. For the deterministic system, it is possible to explore the synchronized state analytically by solving the equation of motion in all the possible states of the two potentials and propagating the initial conditions.

The general solution of the equation of motion (Eq. **1** in main text) is $x_\pm(t) = x_\pm(0)\exp(-t/\tau_\pm)$, where $x_\pm = x_2 \pm x_1$ and x_1, x_2 are the displacements of the two beads about their reference positions, and we take $\tau_\pm = \tau_0(1 \pm 3a/2d)^{-1}$ assuming for simplicity that the particles are at fixed distance d along the x axis (in our case this is a better approximation than fixing their distance as the equilibrium position of their potential in each of the four possible states of the potentials).

We will call $\epsilon = 3a/2d$ and use it to quantify the strength of the hydrodynamic coupling. The most instructive results can be obtained by considering the effect of small perturbations at weak coupling strength. Let us consider a perturbation from the antiphase state, i.e. we start from the configuration where particle 1 has displacement $x_1(0) = -\rho$ and particle 2 starts from a displaced position $x_2(0) = r < \rho$, where we have called $\rho = \lambda - \xi$ (this is measured relative to the minimum of the second potential). The switches for the two particles are at $\mp\xi$. Note that

with our convention, the equilibrium point of the potentials is always at zero displacement.

We call $h = 1 - r/\rho$ the normalized displacement with respect to the antiphase state at time $t = 0$, and we compute the propagation of h after a cycle of the dynamics. We will assume that h is of order ϵ.

STEP 1: We have to compute the time $\bar{t}$ before the first switch (when particle 2 reaches position ξ) and the position $-x_{1s}$ of the first particle when this occurs. For $h = 0$ the relaxation involves only x_- and thus $\bar{t} = \tau_- \log(\rho/\xi)$ and $x_{1s} = \xi$. For general h, one has to solve the equations:

$$2\xi = (r - \rho)\exp(-\bar{t}/\tau_+) + (r + \rho)\exp(-\bar{t}/\tau_-),$$
$$2x_{1s} = (\rho - r)\exp(-\bar{t}/\tau_+) + (r + \rho)\exp(-\bar{t}/\tau_-). \quad \textbf{[S3]}$$

For $\bar{t}$ and x_{1s}. These can be solved in a straightforward way with a perturbative expansion in ϵ and h.

STEP 2: The procedure is then iterated, and one has to solve the same problem with new initial conditions (resetting $t = 0$ as the initial time) $x_1(0) = -x_{1s}$ and $x_2(0) = r < -\rho$ (thus in this step the particles feel a force in the same direction). Similar equations as above can be used to determine the switch time for particle 1 and the switch position x_{2s}. These two calculation steps are sufficient, as the third and fourth substeps of the cycle are formally symmetric to the first two.

For each semicycle we find that the initial perturbation h maps into the perturbation:

$$h' = h[1 - \epsilon B(\rho, \xi)], \quad \textbf{[S4]}$$

where

$$B(\rho, \xi) = \frac{\rho^2 - \xi^2}{\rho\xi} + 2\log\frac{\rho}{\xi}. \quad \textbf{[S5]}$$

Note that for our geometrical choice of the parameters $B > 0$ always, proving the stability of the antiphase mode. Perhaps surprisingly, the linear corrections to the perturbation are irrelevant, and the first relevant corrections are to second order in ϵ.

An analogous result holds for the instability of the inphase state.

One can use the result of Eq. **S4** to make a prediction for the correlation time of the phase difference observed in the experiments. Rewriting the evolution equation for h as $\dot{h} = -\epsilon B h$, where the dot indicates a discrete derivative and the time unit is half a cycle, it is evident that this variable should relax exponentially with the characteristic time (in half cycles) of $(B\epsilon)^{-1}$. This prediction fits reasonably well the observed behavior in the experiments, as can be seen in Fig. S3 where in particular the linear increase with d is confirmed.

We have also obtained the full map $r'(r)$ relating any arbitrary initial condition of the system, which is not very transparent. However it can be written explicitly and explored numerically. We have performed this analysis, which confirms that the antiphase state is the only stable one. It is also possible to verify using the full map that the inphase and antiphase state are fixed points of the dynamics.

Going back to the equation for the normalized displacement from the antiphase state,

$$\dot{h} = -\epsilon B h,$$

we would like to point out that this equation is directly comparable to the effective equation for the phase difference that is sometimes used in the context of synchronizing oscillators (4, 5).

In our system, since the dynamics is governed by the geometric switch mechanism and not by an intrinsic phase variable, there is no natural definition of instantaneous phase difference. However, the normalized perturbation from the antiphase state is naturally measured at the switch time by monitoring the positions of the two beads. More specifically, we can compare this equation to the analogous one for the model for cilia by Niedermayer and coworkers (6). In this model, cilia are represented as hydrodynamic beads in rotary motion on an orbit of harmonically deformable radius, and reach an inphase synchronized state. The above equation indicates that, in the case of equal intrinsic frequencies, the relaxation of dynamics of the two models is identical. Indeed, in both models, the characteristic relaxation time to the synchronized state in cycles is inversely proportional to ϵ times a parameter (in our case B) depending on geometric features of the single oscillator and affecting its natural beating time.

When the two oscillators' intrinsic frequencies differ slightly, $\kappa_2 = \kappa_1(1 + q)$, with small q, the behavior of the two models also appears to be similar. The deterministic simulations indicate that in presence of a small q, the synchronized (antiphase, in our case) fixed point is linearly displaces by detuning. Analytically, supposing that the oscillation will be dominated by the mode x_- as it happens for $q = 0$, we can estimate the value of the fixed point for h by considering a small deformation of the mode. By this procedure we obtain the following effective equation for h

$$\dot{h} = \frac{q}{2}(1 + \epsilon) - \epsilon B h,$$

which confirms the linear effect of detuning that is observed in deterministic simulations.

Difference in Arrival Time for Two Beads in Stationary Potentials. Using numerical simulations we show here that a finite delay time is already present in the simpler situation of two beads in stationary potentials. Namely, we consider two beads confined by harmonic traps centered at distance d, starting from opposite initial displacements $\pm(\lambda - \xi)$ from their equilibrium positions, as sketched in Fig. S6. We record their arrival times t_1 and t_2 at displacements $\pm\xi$ for many realizations and we consider the histogram of $|\Delta t| = |t_1 - t_2|$. Fig. S7 shows that this quantity develops a coupling-dependent (i.e. distance-dependent) peak at a characteristic time well separated from zero. On the other hand, the realization average $\langle t_1 - t_2 \rangle = 0$ as for the delay times for the antiphase state over many cycles. Quantitatively, the two characteristic delay times are not identical, since in the case of antiphase switching in the synchronized state the initial conditions for the two beads are not equal (and not deterministic).

Studying further this simple model, Fig. S7 shows that the hydrodynamic correlation of the stochastic noise is a key factor causing the finite time delay in arrival times between the two particles. In a simulation where the noise term is taken by considering each bead as an isolated particle (a choice that violates the fluctuation dissipation theorem, but is an interesting control to understand the origin of the finite delay result) the maximum probability of arrival is at equal times ($|\Delta t| = 0$).

Further Numerical Results on Detuning. Full results of synchronization with traps of different stiffness, Fig. S2.

Details of Experimental Trajectories in Synchronized State. As described in the text, the trajectories of each bead are composed of segments that are to a good approximation parts of exponential functions. Also to a first approximation (absence of noise) the trajectories are in antiphase when there is synchronization. Plotting $x_1(t)$ vs $x_2(t)$ would give a line of gradient 1 for inphase, and gradient -1 for antiphase motion. These are orbits. In the presence of thermal noise, there is a stochastic delay between the switch times of the two beads, and the orbits acquire more structure.

The order parameter Q presented in the text and in the *Methods* section is a good way to quantify the fraction of time

that beads oscillate in phase or in antiphase, but a finer analysis is required to explore the structure of orbits in the presence of noise.

In a full cycle, there are two trap moves of trap 1 (+ and −) and two moves for trap 2 (+ and −). For orbits that are close to phase or antiphase there will be pairs of moves, separated by a longer time during which the beads relax towards the potential minima. There are only eight possible sequences of moves to form a cycle, taking trap 1 moving right as the first move. This is excluding "quick" return moves of the same particle. Labeling 1+ the trap 1 to the right move, 1− trap 1 to left, 2+ and 2− similarly for trap 2, and P as the long time between moves, these sequences are listed in Table S1. Pairs of sequences are identical under time symmetry (switch of all + and −).

This analysis is applied to the experimental data obtained over various values of d. Fig. S1 shows the histogram of each orbit type described above, at various d. This confirms the prevalence of ring-shaped orbits and antiphase motion, although with increasing thermal noise relative to coupling strength there is an increasing amount of all types of orbit.

1. Leoni M, Kotar J, Bassetti B, Cicuta P, Cosentino Lagomarsino M (2009) A basic swimmer at low reynolds number. *Soft Matter* 5:472–476.
2. Ermak DL, McCammon JA (1978) Brownian dynamics with hydrodynamic interactions. *J. Chem. Phys* 69:1352–1360.
3. Meiners JC, Quake SR (1999) Direct measurement of hydrodynamic cross correlations between two particles in an external potential. *Phys Rev Lett* 82:2211–2214.
4. Pikovsky A., Rosenblum M, Kurths J (2001) *Synchronization* (Cambridge Univ. Press, Cambridge, U.K.).
5. Kuramoto Y (1975) International symposium on mathematical problems in theoretical physics. *Lecture Notes in Physics*, ed Araki H (Springer, Berlin), Vol 39.
6. Niedermayer T, Eckhardt B, Lenz P (2008) Synchronization, phase locking, and metachronal wave formation in ciliary chains. *Chaos* 18:037128.

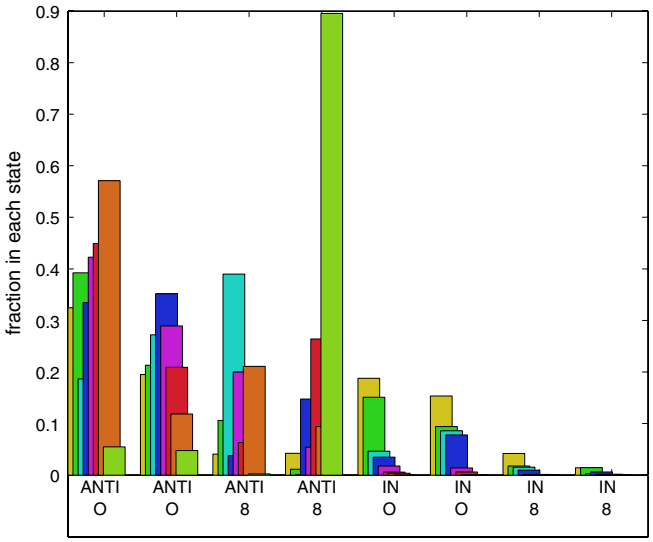

Fig. S1. Distribution of the types of orbits observed over a long experimental run. Bars of different colors correspond to different distances, with the values of $d = [4, 6, 8, 10, 15, 20, 30, 40]$ μm from left to right. The classification of orbits is done to distinguish phase from antiphase, and orbits of x_1 vs x_2 that are topologically ring-shaped vs orbits that are 8-shaped. This analysis confirms the dominance of antiphase behavior, and of ring-shaped orbits. For large d, the synchronization is lost and at the same time the orbits topology becomes random.

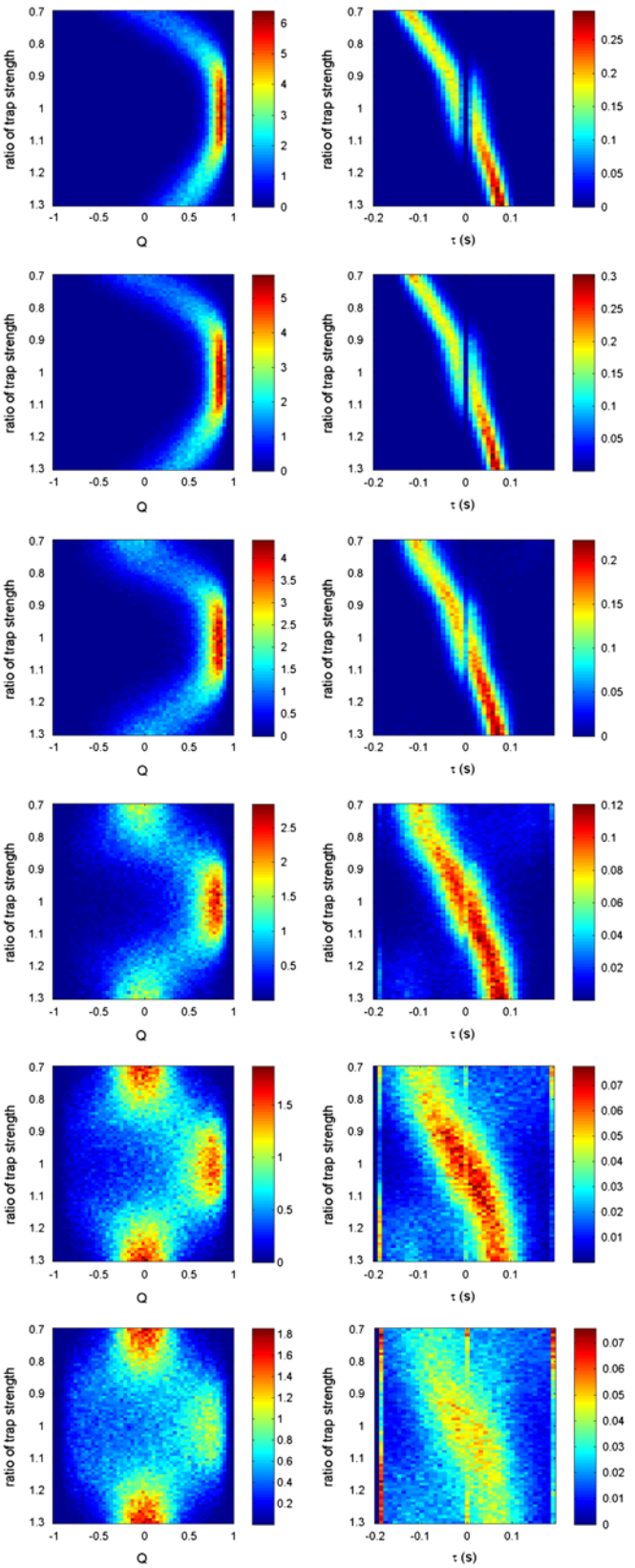

Fig. S2. Distribution of the synchronization parameter Q and of Δt when the trap stiffness ratio is varied (numerical data), for the distances $d = [4, 5, 8, 16, 32, 64]$ from top to bottom.

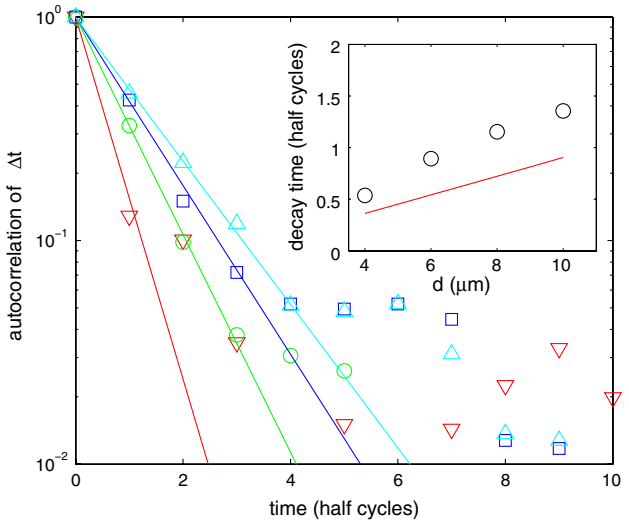

Fig. S3. The experimental autocorrelation of the difference in arrival times Δt decays exponentially. In the figure this quantity is plotted for experimental antiphase states at different distances. Solid lines are best fits. The inset shows the decay times as a function of d increasing linearly in qualitative agreement with Eq. **S4** (solid line).

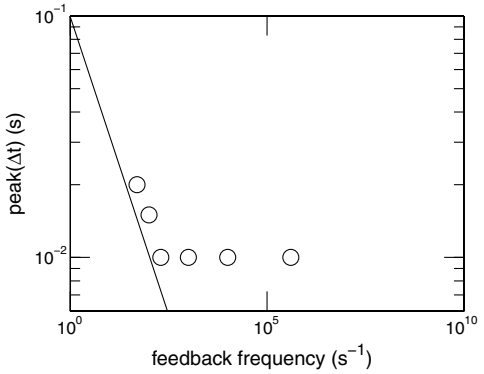

Fig. S4. Average of absolute switch time delay of two beads at $d = 5$ μm. Figure shows that the system has a characteristic delay time which is independent of the feedback time, provided that this is sufficiently short (i.e. high feedback frequency). The system parameters in this simulation are $\kappa = 2$ pN/m, $\eta = 7.5$ mPa s. Markers are the peak position of Δt, and the solid line is $y = 1/x$.

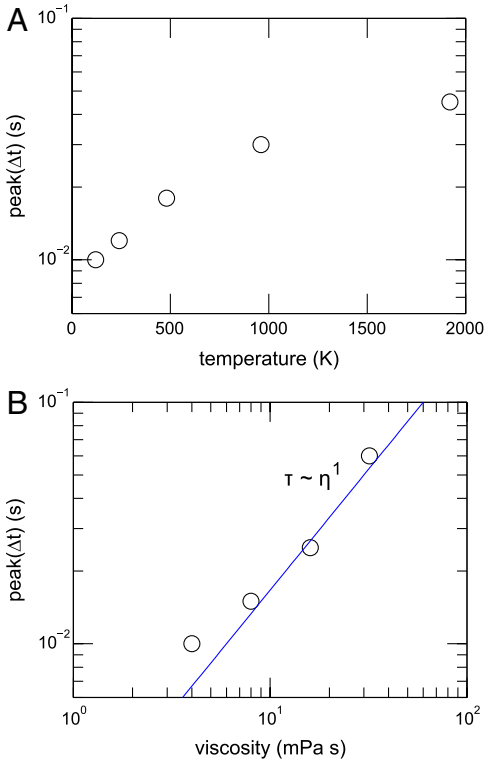

Fig. S5. Movement of the peak value of the Δt distribution as a function of temperature (*A*) and viscosity (*B*). Trends show an exponential dependence of peak(Δt) at low *T*. As a function of viscosity the linear scaling is not surprising, since viscosity sets the timescale of the experiment. The same trends are seen also for $<|\Delta t|>$. The system parameters in this simulation are $d = 5$ μm, $a = 1.5$ μm, $\lambda = 1$ μm, $\kappa = 2$ pN/m. In (*A*), the viscosity is $\eta = 7.5$ mPa s, while in (*B*) the temperature is $T = 23C$.

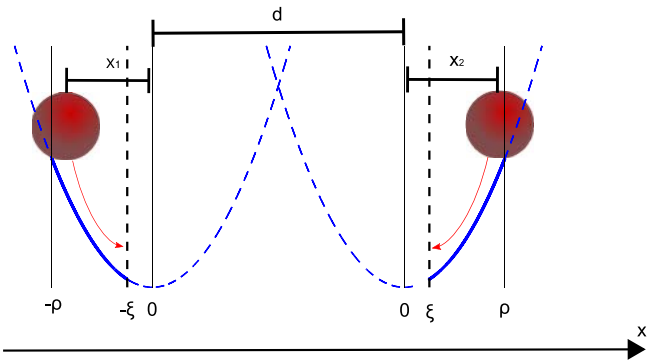

Fig. S6. The finite values of Δt that are seen with synchronization are also a feature of a simpler system. The diagram shows the simpler scenario that has been studied numerically, where at time $t = 0$ two beads are initially placed at opposite ("antiphase") positions in two harmonic wells a distance *d* apart. The beads fall towards the minimum, and hydrodynamic correlations develop. The times of first passage of bead 1 and 2, respectively, at $-\xi$ and $+\xi$ are recorded. Then many realizations of the stochastic simulation build up a distribution of first passage times. No "switch" of the potential takes place in this simple scenario.

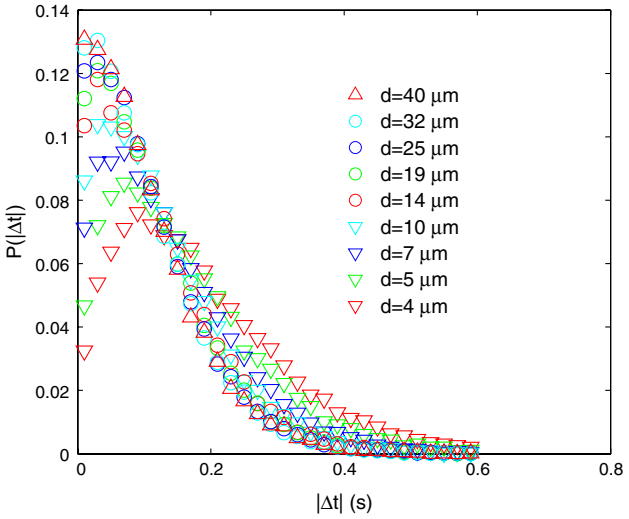

Fig. S7. The arrival times of two particles starting from opposite positions in harmonic potentials a distance d apart are anticorrelated. This is a simpler situation than in the synchronized state studied in the main text, since here the initial position of the particles is set. The histograms show the distribution of the difference in time of arrival, obtained in numerical simulation. The parameters used for this figure are $\eta = 3.55 \times 10^{-3}$ Pa s, $\kappa = 0.428$ pN/μm, $a = 1.735$ μm, $T = 296$ K, $\xi = 0.25$ μm, $\rho = 0.75$ μm. No feedback time.

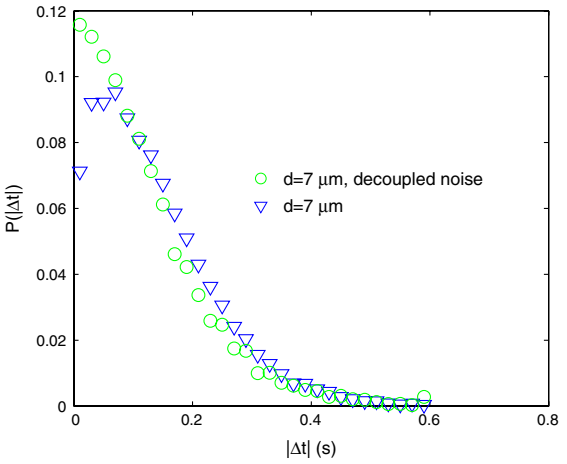

Fig. S8. The dip in the probability distribution of arrival time intervals disappears if the thermal noise is not taken with the correct correlation property. The parameters used in the simulation for these data are the same as in Fig. S7, except that there is no interparticle correlation in the noise term included in the equations of motion that generate the data shown with (○) markers. It should be noted that the only noise term that respects the fluctuation dissipation theorem is the one with the correct correlation property.

Table S1. Possible sequences of moves to form a cycle

Sequence	Type	Topology
1+ 2- P 1- 2+ P	antiphase	ring
1+ P 2+ 1- P 2-	antiphase	ring
1+ P 1- 2+ P 2-	antiphase	8
1+ 2- P 2+ 1- P	antiphase	8
1+ P 2- 1- P 2+	phase	ring
1+ 2+ P 1- 2- P	phase	ring
1+ 2+ P 2- 1- P	phase	8
1+ P 1- 2- P 2+	phase	8

Move labels are explained in *SI Text*.